Journal of Solid State Chemistry **164,** 188–200 (2002)
doi:10.1006/jssc.2001.9457, available online at http://www.idealibrary.com on IDEAL®

Defect Analysis of Ionically Compensated Quadruple and Quintuple Perovskite Layered Cuprates with Ti Blocking Layers

N. Mansourian-Hadavi,[1,*] T. O. Mason,* D. Ko,‡ and K. R. Poeppelmeier†

*Materials Science and Engineering Department, Northwestern University, 2225 North Campus Drive, Evanston, Illinois 60208-3108; †Department of Chemistry, Northwestern University, Evanston, Illinois, 60208-3113; and ‡Technology Development Center, Rubicon Technology Inc., 3000 Lakeside Drive, Suite 105N, Bannockburn, Illinois 60015

Received July 17, 2001; accepted November 16, 2001; published online February 1, 2002

This work presents a modified defect model for pure and chemically substituted quadruple and quintuple pure perovskite layered cuprates, using data from the Jonker (thermopower vs ln conductivity) and Brouwer (log conductivity vs log pO_2) analyses. The closely matched in-plane bond lengths of the blocking and the active layers in these structures promote ionic compensation rather than electronic compensation upon aliovalent *p*-type doping. A comprehensive defect model that takes into account all the major defect species in an ionically compensated quadruple or quintuple perovskite provides a better means for understanding the electrical behavior of these novel materials. The presented model allows for the calculation of effective dopant and the oxygen interstitial concentrations in these materials. © 2002 Elsevier Science (USA)

INTRODUCTION

Quadruple and quintuple perovskite layered cuprates are novel members of the layered cuprate family of compounds. Because they have in common with high-T_c superconductors certain structural features (e.g., 2D copper–oxygen sheets), they have been extensively studied. In particular, the defect chemistry of layered cuprates is of interest insofar as doping/carrier generation mechanisms are concerned (1–9). Carrier generation is a necessary, but not sufficient, step for achieving high-T_c superconductivity. Previous point defect models for layered cuprates are overly simplified, and do not appropriately account for the high degree of ionic compensation that takes place in quadruple and quintuple perovskite cuprates. The present work develops an improved model and applies it to the analysis of high-temperature electrical conductivity and thermopower data in a variety of pure and chemically substituted copper-based quadruple and quintuple perovskites.

[1]To whom correspondence should be addressed. Fax: 847-491-7820. E-mail: n-mansourian@nwu.edu.

Quadruple and quintuple perovskite layered cuprates have double copper–oxygen planes (conducting layer) that are separated by two and three titanate perovskite layers (blocking layer), respectively. A fixed valence and coordination-preferring *B*-cation (e.g., Ti) provides minimal non-stoichiometry in the compounds. They primarily control the doping of the CuO_2 planes by imparting the proper strain (i.e., compressive or tensile) through bond mismatch. Goodenough and Manthiram stressed the importance of the bond length mismatch between the blocking and conducting layers for doping in layered cuprate superconductors (10). The simple schematic in Fig. 1 expresses the bond mismatch idea by comparing the unrelaxed bond lengths of blocking and active layers of common high-T_c layered cuprates with different coordination environments by using Shannon's anion and cation radii (11). In *p*-type superconductors, blocking layers have shorter in-plane bond lengths than the conducting layers since Cu has 5- or 6-fold coordination, with a longer natural Cu–O distance than the *M*–O (M = La, Tl, Hg, etc.) distance in the blocking layer. La_2CuO_4 is an example of such structures that combines La(VI)–O blocking layers ($r \sim 1.84$ Å) with Cu(VI)–O ($r \sim 2.13$ Å) conducting layers. This clearly imparts a compressive strain to the conducting layers as a result of the bond mismatch. On the other hand, in the *n*-type superconductor, $(Nd,Ce)_2CuO_{4-\delta}$, a Nd–O blocking layer ($r \sim 2.04$ Å) is stacked with a Cu(IV)–O conducting layer ($r \sim 1.95$ Å) which imparts a tensile strain to conducting layers. However, structures with Ti–O (perovskite) and Cu(V)–O (e.g., quadruple perovskite layered cuprate $Ln_2Ba_2Cu_2Ti_2O_{11}$) do not have as much bond length differences, resulting in a bond-matched structure. The in-plane bond length for *p*-type superconductors ranges from 1.90 Å to 1.938 Å and for *n*-type superconductors from 1.96 to 1.98 Å leaving a so-called "neutral" region (r_{Cu-O} = 1.938–1.965 Å) in between for bond-matched materials such as quadruple and quintuple layered cuprate perovskites.

0022-4596/02 $35.00

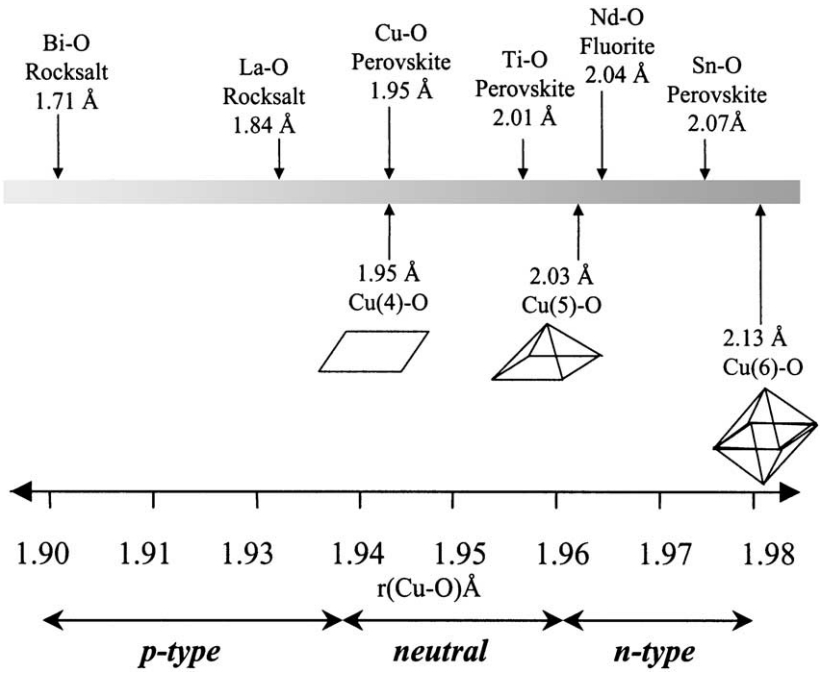

FIG. 1. Schematic presentation for comparison of unrelaxed bond lengths of active and blocking layers of layered cuprate superconductors, using Shannon ionic radii (2) and the range of in-plane bond lengths for *p*- and *n*-type high-T_c superconductors as well as quadruple and quintuple perovskite layered cuprates.

The most important feature of the blocking layer, the fixed oxygen stoichiometry, allows investigation of the active layer properties across a series, since the in-plane bond length in the active layer varies with the composition of the blocking layer. Aliovalent doping in a *p*-type layered cuprate perovskite results in the oxidation of copper in the conducting layer. Acceptor doping of the blocking layer in a compressive structure stabilizes holes while donor doping of the blocking layer in a tensile structure stabilizes electrons in the conducting layer. The extent of aliovalent doping in the blocking layer of a layered cuprate compound depends primarily on the relative host and substituent cationic sizes. The materials with in-plane *M*–O distance in their blocking layer very close to the in-plane Cu–O distance in their conducting layer do not have the necessary driving force (i.e., strain) in their structure to create significant carrier concentration (e.g., $Ln_2Ba_2Cu_2Ti_2O_{11}$). Therefore, aliovalent doping in the bond-matched quadruple and quintuple layered cuprate perovskite compounds results in ionic compensation rather than electronic compensation. However, appropriate *p*-type substitution in *A*- and *B*-sites produces shorter in-plane bond lengths.

Because there are several major defect reactions going on in an aliovalently doped quadruple or quintuple perovskite, a defect model that considers multiple defect regimes allows for better understanding of the defect behavior of the compound. Such a defect model reveals the dominant defect reaction, providing information on the effective dopant level. Oxygen defects are the most common types of defects in the layered cuprate structures. Therefore, the oxygen content of a layered cuprate perovskite can be an indication of its defect concentration. A layered cuprate perovskite with oxygen-deficient blocking or active layers has oxygen vacancies that may or may not be refillable upon subsequent annealing. For example, *B*-site acceptor doping in $La_2Ba_2Cu_{2+x}Ti_{2-x}O_{11-\delta}$ results in oxygen vacancies in the blocking layer according to

$$CuO + Ti_{Ti}^{\times} + O_O^{\times} \rightarrow Cu_{Ti}'' + V_O^{\bullet\bullet} + TiO_2. \qquad [1]$$

Refilling these vacancies introduces holes back to the system:

$$\frac{1}{2}O_2(g) + V_O^{\bullet\bullet} \rightarrow O_O^{\times} + 2h^{\bullet}. \qquad [2]$$

The other recognized oxygen defect reaction in layered cuprates is the formation of oxygen interstitials,

$$\frac{1}{2}O_2(g) \rightarrow O_i'' + 2h^{\bullet}, \qquad [3]$$

which should increase the hole content. However, the formation of oxygen interstitials between adjacent Cu–O sheets is believed to destroy the structural role of these sheets in conductivity (12), although it increases hole concentration and introduces some metallic behavior to the semiconductor.

In an oxygen-deficient material, overall oxygen content can be used to calculate the carrier concentration of the system, assuming that other defects such as interstitials can be ignored. This is the common method to determine the hole content (p) of known superconductors, since the oxygen content directly reflects the true oxidation level of Cu ions. Applying the same method, p is calculated for the ionically compensated acceptor-dopedquadruple or quintuple perovskites in the present study (e.g., $NdDyBa_2Cu_{2.2}Ti_{1.8}O_{11-\delta}$) according to

$$2[V_O^{\bullet\bullet}] + p = 2[Cu''_{Ti}]. \qquad [4]$$

However, unlike an optimally doped layered cuprate superconductor, the calculated p from the above equation does not reflect the true carrier concentration of the compound, if other defect species (e.g., oxygen interstitials) are present. Oxygen annealing treatment of these compounds may enhance electronic and transport properties by partially refilling the oxygen vacancies created by ionic compensation, following the mechanism of Eq. [2]. Prior efforts to refill such vacancies by various oxygen treatments have been partially successful (13–15). This hole generation mechanism is preferred over that of Eq. [3], since deleterious oxygen interstitials are avoided.

The defect model in the present work is based on an earlier defect model developed by Kane *et al.* (9) for undoped quintuple layered cuprate perovskites, using the data from high-temperature thermopower and conductivity measurements (Jonker analysis) and transport properties as a function of oxygen partial pressure (Brouwer analysis). Jonker analysis is a particularly useful method for analyzing the electrical properties of layered cuprates (16). This method has been used for characterization of oxide semiconductors and superconductors in their normal states (17).

The technique consists of plotting thermopower versus the natural logarithm of conductivity, which has a characteristic "pear" shape as illustrated in Fig. 2 (Jonker pear). The conductivity (σ) and thermopower (Q) of a semiconductor are related to transport parameters by

$$\sigma = \sigma^+ + \sigma^- = pe\mu_h + ne\mu_e. \qquad [5]$$

$$Q = \frac{k}{e}\left(\ln\frac{N_v}{p} + A\right) = \frac{Q^+\sigma^+ + Q^-\sigma^-}{\sigma^+ + \sigma^-}, \qquad [6]$$

where p and n are the hole and electron concentrations, μ_h and μ_e are their respective mobilities, e is electron charge, k is Boltzmann's constant, N_v is density of states, and A is a transport parameter (17). The detailed mathematical explanation of Jonker analysis and its usefulness for interpreting electrical properties (i.e., transport properties, bandgap, mobility, density of states, and intrinsic conductivity) are given in the original work (16). An interesting feature of the Jonker pear is that the sign of the thermopower is the same as the sign of the majority carrier. Carrier concentration increases clockwise around the pear for holes and counterclockwise for electrons. The three regions of the pear are demonstrated in Fig. 2. The low-conductivity side corresponds to the intrinsic regime, where both electrons and holes contribute to the electrical properties and the thermopower changes rapidly with small changes in conductivity. The linear regions on the high conductivity side of the diagram are the extrinsic regions, where a single type of carrier contributes to the conductivity and thermopower. The slopes of these legs are $-k/e$ for p-type and $+k/e$ for n-type systems (k is Boltzmann's constant and e is the unit of electronic charge). A transition from intrinsic behavior to hole-doped extrinsic behavior is observed as the copper–oxygen sheets of the insulating parent compounds are hole-doped by cation doping or oxygenation. The data for superconducting compounds fall toward the high-conductivity intercept (low thermopower values) and often exhibit a deviation from linearity, indicating a transition from semiconducting to metallic behavior (heavily doped). The location and size of the pear, the region of the curve where the data falls, and also the spread of the data as a function of oxygen partial pressure or chemical substitution provide substantial information about the defect chemistry and transport properties of a given material.

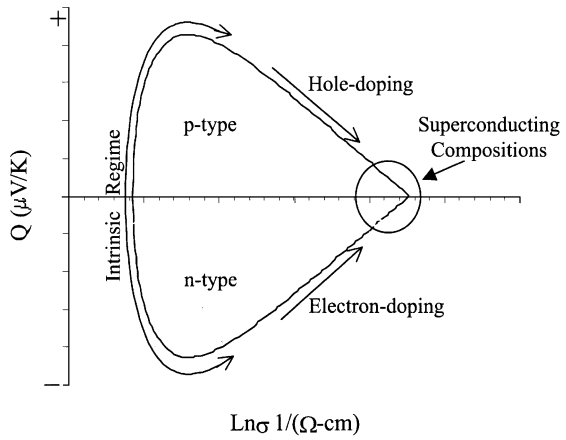

FIG. 2. Jonker plot, after Ref (16).

A Brouwer diagram (Kröger–Vink diagram) is a log–log plot of defect species' concentration vs oxygen partial pressure or doping level. This technique is a standard way to analyze the electronic and defect behavior of oxide systems (18). Since thermopower and conductivity will often track with the majority electronic species according to Eqs. [5] and [6], a log conductivity–log pO_2 or thermopower–$1/T$ plot can provide useful information about the pO_2 or temperature dependence of dominant electronic species.

Since the electrical measurements in the present work were undertaken in a narrow range of oxygen partial

pressure (10^{-5}–1 atm), it was not possible to plot a complete Brouwer diagram that covers all the different defect regimes. However, log conductivity–log pO_2 plots for oxide materials in this work can exhibit prevailing defect regimes under the experimental conditions.

The majority of defect reactions in layered cuprate perovskites are the ones that create oxygen interstitials or vacancies. In the *p*-type oxides, oxygen interstitials and electron holes are the dominant ones as proposed by Hong (19),

$$\frac{1}{2}\,O_2(g) \leftrightarrow O_i'' + 2h^{\bullet} \qquad [7]$$

$$K_{ox} = \frac{[O_i''] P^2}{PO_2^{1/2}} \qquad [8]$$

under the electroneutrality condition

$$p = 2[O_i''] = (2K_{ox})^{1/3} PO_2{}^{1/6}. \qquad [9]$$

This result indicates a positive slope of 1/6 on a log σ–log pO_2 curve.

EXPERIMENTAL

Samples were prepared, corresponding to the stoichiometry $NdDy_{1-z}(Sr,Ca)_zBa_{2-x}Sr_xCu_{2+y}Ti_{2-y}O_{11-\delta}$, $LaY_{1-z}Ca_zBa_{2-x}Sr_xCu_{2+y}Ti_{2-y}O_{11-\delta}$ (quadruple perovskite) and the stoichiometry $NdDyCaBa_{2-x}Sr_xCu_{2+y}Ti_{3-y}O_{14-\delta}$ (quintuple perovskites). Typically 4–5 grams of samples were prepared by solid state reaction of stoichiometric amounts of Ln_2O_3 (Ln = Nd, Dy, La, Y), ACO_3 (A = Ba, Sr, Ca), CuO, and TiO_2, all of purity above 99.99%, using a Sartorius balance (Brinkmann Instrument, Westbury, NY) with $\pm$ 0.1 mg accuracy. The reagents were ground with a mortar and pestle, and fired in high-density alumina crucibles at 950°C in air for 1 day in order to remove carbonates. Each sample was then ground and pressed at $\sim$ 2 MPa into pellets 12.5 millimeters diameter and 3–5 millimeters thick. The pellets were then fired at 1030–1050°C over the course of a 5–7-day reaction period, with several intermittent regrindings.

The phase purity of the air-quenched polycrystalline samples was determined by X-ray powder diffraction on a Rigaku diffractometer with Ni-filtered Cu$K\alpha$ radiation. Data were collected from 10° to 80° 2θ with a step size of 0.05° and a collection time of 2 seconds at each step. Silicon was used as an internal standard. Lattice parameters were determined by pattern matching [Le Bail fitting (20)] based on a tetragonal unit cell ($P4/mmm$). The fitting was made with the GSAS program (21).

To determine the oxygen stoichiometry and average copper valence in the samples, hydrogen reduction thermogravimetry was performed (TA Instrument 2950, New Castle, DE). Oxygen annealing of the samples was performed prior to TGA analysis, by equilibrating in flowing oxygen at 900°C and then slowly cooling to room temperature (< 1°C/min) to facilitate oxygen trapping in the oxide structure. For TGA runs, samples were preheated at 120°C for 2 hours to remove any possible moisture. They were then heated to 900°C at the rate of 5°C/min, isothermally maintained for 10 hours, and then cooled to room temperature. The whole process was carried out in a 7% H_2/N_2 mixture to achieve the desired reduction.

Simultaneous four-point DC conductivity and Seebeck coefficient measurements, at temperatures from 800 to 650°C, were performed using the technique described previously (22, 23). Rectangular bar-shaped samples (3mm × 3mm × 9mm) were cut from sintered pellets and placed between Au foils, the outer electrodes for electrical measurements, with auxiliary Au wire electrode contacts at $\sim\frac{1}{3}$ and $\sim\frac{2}{3}$ positions along each bar. A Pt and Pt/Rh thermocouple (type S) was placed in contact with each of the four electrodes along the bar. Samples were equilibrated in oxygen partial pressures ranging from 10^{-5} atm to 1 atm using oxygen or oxygen–argon premixtures. Measurements were taken after equilibrium had been achieved (6–10 hours). Conductivity/thermopower data were also taken during slow-cooling over the temperature range, 800 to 400°C, under flowing pure oxygen at a cooling rate of 20°C/hour. The measured conductivities were corrected for the porosity of the samples according to the asymmetric medium equation in the work of McLachlan *et al.* (relative density of 70%–75%) (24).

RESULTS AND DISSCUSION

The previous studies on several quadruple and quintuple perovskites layered cuprates ($NdDyBa_{2-x}Sr_xCu_{2+y}Ti_{2-y}O_{11-\delta}$, $LaY_{1-z}Ca_zBa_2Cu_{2+y}Ti_{2-y}O_{11-\delta}$, and $NdDyCaBa_{2-x}Sr_xCu_{2+y}Ti_{3-y}O_{14-\delta}$) elucidated their unique electrical properties and defect chemistry of these materials (9, 15, 25). The new *A*- and *B*-site doped $NdDy_{1-z}(Ca,Sr)_zBa_{2-x}Sr_xCu_{2+y}Ti_{2-y}O_{11-\delta}$ and $LaY_{1-z}Ca_zBa_2Cu_{2+y}Ti_{2-y}O_{11-\delta}$ quadruple compounds were prepared based upon promising properties of these families of material (bond lengths, conductivity, and thermopower) in prior work (15). X-ray diffraction analysis detected no impurity phases in $NdDy_{1-z}Sr_zBa_2Cu_{2+y}Ti_{2-y}O_{11-\delta}$ for $0 \le z \le 0.2$ and $0 \le y \le 0.2$, $LaY_{1-x}Ca_xBa_2Cu_2Ti_2O_{11-\delta}$ for $0 \le x \le 0.5$, $LaY_{1-x}Ca_xBa_2Cu_{2.2}Ti_{1.8}O_{11-\delta}$ for $0 \le x \le 0.3$, and $NdDy_{0.9}Ca_{0.1}Ba_{1.5}Sr_{0.5}Cu_{2.2}Ti_{1.8}O_{11-\delta}$. Employing the small–large $A'A''$ cation combination such as Nd and Dy or La and Y in these quadruple compounds is a strategy to prevent the incorporation of oxygen defect species between adjacent copper–oxygen layers (25, 26). This design reduces the spacing between adjacent Cu–O layers, making oxygen intercalation energetically unfavorable. *A*- and *B*-site aliovalent codoping ($[Sr'_{Dy}]$, $[Ca'_Y]$, $[Cu''_{Ti}]$) was the primary

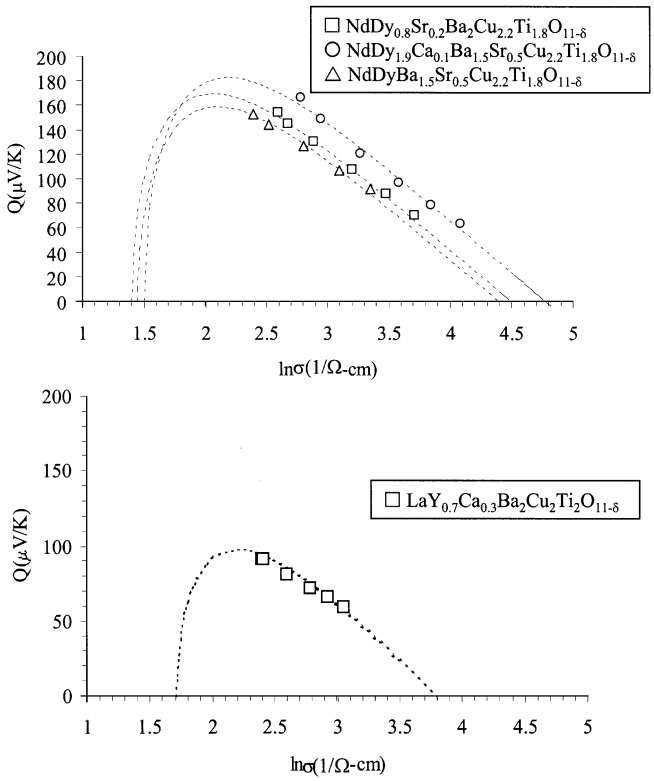

FIG. 3. Jonker plots for quadruple perovskites at 700°C. Oxygen partial pressures increase clockwise around the pear at values of 10^{-5}, 10^{-4}, 10^{-3}, 10^{-2}, 10^{-1}, and 1 atm.

strategy to increase the hole concentration of the systems. Low-temperature resistivity measurements showed, however, no superconducting transition in these quadruple compounds.

TABLE 1
Lattice Parameters for $NdDy_{1-z}(Sr,Ca)_zBa_{2-x}Sr_xCu_{2+y}Ti_{2-y}O_{11-\delta}$ Quadruple Compounds, Refined by GSAS Program

Compound	a (Å)	c (Å)
$NdDy_{0.9}Sr_{0.1}Ba_2Cu_2Ti_2O_{11-\delta}$	3.8898 ± 0.0004	15.690 ± 0.002
$NdDy_{0.8}Sr_{0.2}Ba_2Cu_2Ti_2O_{11-\delta}$	3.8948 ± 0.0003	15.701 ± 0.001
$NdDy_{0.7}Sr_{0.3}Ba_2Cu_2Ti_2O_{11-\delta}$	3.8946 ± 0.0004	15.678 ± 0.002
$NdDy_{0.6}Sr_{0.4}Ba_2Cu_2Ti_2O_{11-\delta}$	3.9002 ± 0.0005	15.679 ± 0.002
$NdDy_{0.8}Sr_{0.2}Ba_2Cu_{2.2}Ti_{1.8}O_{11-\delta}$	3.8953 ± 0.0004	15.692 ± 0.002
$NdDy_{0.7}Sr_{0.3}Ba_2Cu_{2.2}Ti_{1.8}O_{11-\delta}$	3.8956 ± 0.0003	15.693 ± 0.001
$NdDy_{0.8}Sr_{0.2}Ba_{1.5}Sr_{0.5}Cu_{2.2}Ti_{1.8}O_{11-\delta}$	3.8977 ± 0.0005	15.659 ± 0.001
$NdDy_{0.9}Ca_{0.1}Ba_{1.5}Sr_{0.5}Cu_{2.2}Ti_{1.8}O_{11-\delta}$	3.9002 ± 0.0002	15.725 ± 0.003
$LaYCaBa_2Cu_{2.2}Ti_{1.8}O_{11-\delta}$	3.9010 ± 0.0005	15.705 ± 0.005
$LaY_{0.9}Ca_{0.1}Ba_2Cu_2Ti_2O_{11-\delta}$	3.8971 ± 0.0008	15.702 ± 0.003
$LaY_{0.8}Ca_{0.2}Ba_2Cu_2Ti_2O_{11-\delta}$	3.8961 ± 0.0002	15.703 ± 0.001
$LaY_{0.7}Ca_{0.3}Ba_2Cu_2Ti_2O_{11-\delta}$	3.8982 ± 0.0003	15.706 ± 0.001
$LaY_{0.6}Ca_{0.4}Ba_2Cu_2Ti_2O_{11-\delta}$	3.9011 ± 0.0003	15.704 ± 0.002
$LaY_{0.5}Ca_{0.5}Ba_2Cu_2Ti_2O_{11-\delta}$	3.9039 ± 0.0004	15.709 ± 0.002

The in-plane bond lengths of these compounds (Table 1) fall in the neutral region of Fig. 1. Therefore, the bond-matched character of their structure provides no driving force for the formation of carriers as a strain reliever. Such a behavior leads to a low carrier concentration (see below), because ionic compensation becomes the dominant compensation mechanism as opposed to the desired electronic compensation.

Thermogravimetric Analysis

The oxygen contents of the oxygen-annealed $NdDyBa_{2-x}Sr_xCu_{2+y}Ti_{2-y}O_{11-\delta}$ and $LaY_{1-z}Ca_zBa_2Cu_{2+y}Ti_{2-y}O_{11-\delta}$ quadruple perovskite samples were measured using TGA analysis (Table 2). The TGA-derived hole content (p') in Table 2 is calculated according to Eq. [4] based on the common method used to derive the oxidation level of Cu in known layered cuprate superconductors, as discussed before. In other words, if we assume that oxygen interstitials are not present in significant concentration, the oxygen content should be representative of the carrier concentration. For example, $\delta = 0.2$ (oxygen content = 10.8) in $NdDyBa_{2-x}Sr_xCu_{2.2}Ti_{1.8}O_{11-\delta}$ corresponds to strictly divalent copper, which is the result of ionic rather than electronic compensation. Larger oxygen contents (smaller δ) for $x > 0$ suggest that the smaller Sr substituted for Ba ion may make oxygen vacancy refilling easier (15). However, in these *B*-site doped quadruple compounds, where ionic compensation dominates, most of the acceptor species, $[Cu''_{Ti}]$, exist in neutral associates of $[(Cu''_{Ti}V_O^{\bullet\bullet})^{\times}]$; only the residual are effective hole dopants. Hence, the calculation of hole content using Eq. [4] overestimates the carrier content of quadruple perovskites with Ti blocking layers. Later, we will introduce a modified defect model for these compounds that provides a more accurate estimation of Cu oxidation level. Therefore, the "TGA-derived hole content" (p') is used in this paper to distinguish the estimated hole content using the oxygen content (Eq. [4]) vs the estimated hole content considering the overall defect chemistry (p), as described below.

High-Temperature Electrical Characterization

Jonker analysis for the $NdDy_{1-z}(Sr, Ca)_zBa_{2-x}Sr_xCu_{2+y}Ti_{2-y}O_{11-\delta}$ and $LaY_{1-z}Ca_zBa_2Cu_{2+y}Ti_{2-y}O_{11-\delta}$ samples was performed over a range of temperatures and oxygen partial pressures. Figure 3 shows the upper half of the Jonker pear for $LaY_{0.7}Ca_{0.3}Ba_2Cu_2Ti_2O_{11-\delta}$ $NdDy_{0.8}Sr_{0.2}Ba_2Cu_{2.2}Ti_{1.8}O_{11-\delta}$, and $NdDy_{1.9}Ca_{0.1}Ba_{1.5}Sr_{0.5}Cu_{2.2}Ti_{1.8}O_{11-\delta}$ along with the Jonker plot of $NdDyBa_{1.5}Sr_{0.5}Cu_{2.2}Ti_{1.8}O_{11-\delta}$ for comparison purposes. The plots for the *A*-site doped and *A*- and *B*-site codoped quadruple samples in Fig. 3 suggest improvement in electrical properties of the systems upon co-doping, as compared

TABLE 2
Oxygen content for $NdDy_{1-z}Sr_zBa_2Cu_{2+y}Ti_{2-y}O_{11-\delta}$ Quadruple Compounds from TGA Analysis (Hole Contents Are Calculated per Copper Atom)

Compound	Oxygen content	TGA-derived hole content (p')	Oxygen annealed/air quenched
$NdDy_{0.9}Sr_{0.1}Ba_2Cu_2Ti_2O_{11-\delta}$	11.01 ± 0.02	0.10	Oxygen annealed
$NdDy_{0.8}Sr_{0.2}Ba_2Cu_2Ti_2O_{11-\delta}$	10.96 ± 0.02	0.12	Oxygen annealed
$NdDy_{0.7}Sr_{0.3}Ba_2Cu_2Ti_2O_{11-\delta}$	10.92 ± 0.02	0.14	Oxygen annealed
$NdDy_{0.6}Sr_{0.4}Ba_2Cu_2Ti_2O_{11-\delta}$	10.89 ± 0.02	0.18	Oxygen annealed
$NdDy_{0.8}Sr_{0.2}Ba_2Cu_{2.2}Ti_{1.8}O_{11-\delta}$	10.81 ± 0.02	0.22	Air quenched
$NdDy_{0.7}Sr_{0.3}Ba_2Cu_{2.2}Ti_{1.8}O_{11-\delta}$	10.78 ± 0.02	0.26	Oxygen annealed
$NdDy_{0.8}Sr_{0.2}Ba_{1.5}Sr_{0.5}Cu_{2.2}Ti_{1.8}O_{11-\delta}$	1078 ± 0.02	0.07	Oxygen annealed
$LaYBa_2Cu_2Ti_2O_{11-\delta}$	11.01 ± 0.02	0.0	Oxygen Annealed
$LaYCaBa_2Cu_{2.2}Ti_{1.8}O_{11-\delta}$	10.77 ± 0.10	0.0	Air quenched
$LaY_{0.95}Ca_{0.05}Ba_2Cu_2Ti_2O_{11-\delta}$	11.02 ± 0.02	0.09	Oxygen annealed
$LaY_{0.9}Ca_{0.1}Ba_2Cu_2Ti_2O_{11-\delta}$	10.99 ± 0.02	0.040	Oxygen annealed
$LaY_{0.8}Ca_{0.2}Ba_2Cu_2Ti_2O_{11-\delta}$	10.99 ± 0.02	0.095	Oxygen annealed
$LaY_{0.7}Ca_{0.3}Ba_2Cu_2Ti_2O_{11-\delta}$	10.97 ± 0.02	0.120	Oxygen annealed
$LaY_{0.6}Ca_{0.4}Ba_2Cu_2Ti_2O_{11-\delta}$	10.88 ± 0.02	0.085	Oxygen annealed
$LaY_{0.5}Ca_{0.5}Ba_2Cu_2Ti_2O_{11-\delta}$	10.87 ± 0.02	0.116	Oxygen annealed

to the *B*-site doped $NdDyBa_{1.5}Sr_{0.5}Cu_{2.2}Ti_{1.8}O_{11-\delta}$ and $LaYBa_2Cu_{2.2}Ti_{1.8}O_{11-\delta}$ quadruple compounds characterized in previous work (i.e., lower thermopower values and slightly higher σ_{max} intercept) (15, 25). The relatively large values of the conductivity data (σ_{max}) imply that either the density of states near the Fermi level and/or the carrier mobility is enhanced. The fact that data for the *A* and *B*-site doped systems falls more toward the extrinsic leg of the plot compared to that of parent compounds from previous work implies an increased hole content of the system (25).

The slow-cooling plots for the same codoped compounds are shown in Fig. 4 and exhibit thermopower values very close to the threshold of superconductivity ($\sim 43\ \mu V/K$). Semiconducting-to-metallic transition behavior (i.e., deviation of the data from the $-k/e$ slope expected for semiconductors) is also observed. The higher σ_{max} intercept of the $NdDy_{1.9}Ca_{0.1}Ba_{1.5}Sr_{0.5}Cu_{2.2}Ti_{1.8}O_{11-\delta}$ compound, compared to the best *B*-site-only doped sample, $NdDyBa_{1.5}Sr_{0.5}Cu_{2.2}Ti_{1.8}O_{11-\delta}$, indicates enhanced electrical and transport properties.

Brouwer Analysis

The log σ vs log pO_2 plot (at 700°C) for the $NdDy_{1.9}Ca_{0.1}Ba_{1.5}Sr_{0.5}Cu_{2.2}Ti_{1.8}O_{11-\delta}$, $NdDy_{1.8}Sr_{0.2}Ba_2Cu_{2.2}Ti_{1.8}O_{11-\delta}$, and $LaY_{0.7}Ca_{0.3}Ba_2Cu_2Ti_2O_{11-\delta}$ samples,

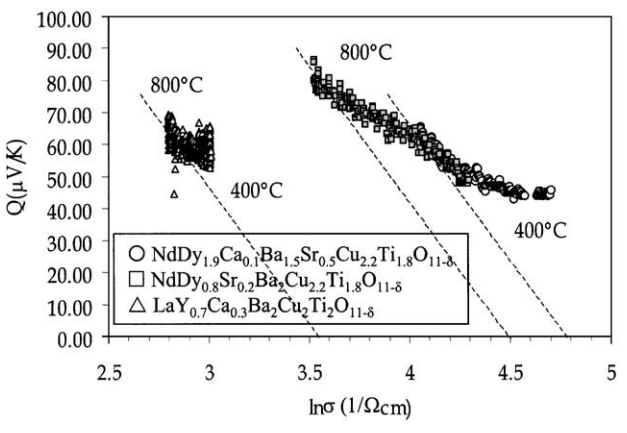

FIG. 4. Simultaneous thermopower–conductivity measurements on slow-cooled quadruple samples at 20°C/hour rate from $\approx$ 800°C to 400°C under flowing oxygen.

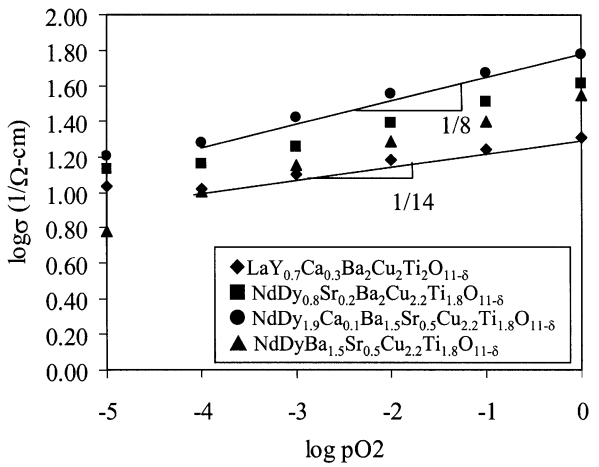

FIG. 5. Brouwer plot of log σ–log pO_2 for quadruple perovskites at 700°C.

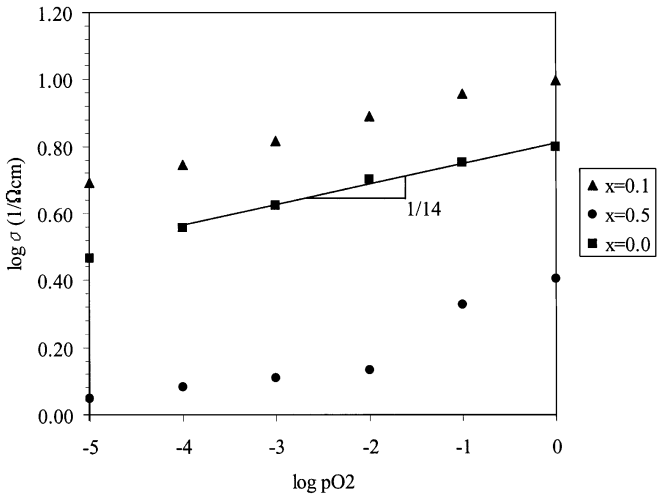

FIG. 6. Plot of log σ–log pO_2 for $NdDyCaBa_{2-x}Sr_xCu_{2.2}Ti_{2.8}O_{14-\delta}$ quintuple perovskite compound at 700°C.

along with the $NdDyBa_{1.5}Sr_{0.5}Cu_{2.2}Ti_{1.8}O_{11-\delta}$ sample as reference from previous work (15) in Fig. 5, indicates a very small pO_2 dependence of conductivity for the LaY quadruple compound ($\sim 1/14$) compared to the rest of the NdDy quadruples with $\sim 1/8$ slopes. This plot shows that the $NdDy_{1.9}Ca_{0.1}Ba_{1.5}Sr_{0.5}Cu_{2.2}Ti_{1.8}O_{11-\delta}$ sample has the highest σ of all the samples. A Brouwer plot for $NdDyCaBa_{2-x}Sr_xCu_{2+2}Ti_{3-y}O_{14-\delta}$ ($x = 0$, 0.1, 0.5) quintuple perovskite compounds using data in previous work (15) is presented in Fig. 6.

The expected slope in log σ–log pO_2 plots of the quadruple and quintuple perovskite systems due to oxygen interstitials as the dominant ionic defect and holes as the major charge carriers (Eq. [9]) is 1/6, as discussed before. The deviation from this calculated value toward smaller slopes in the Brouwer plot in Fig. 5 (~1/14–1/8), with the hint of a plateau at lower oxygen partial pressures, suggests that oxygen interstitials are not the only defect species to be considered.

Since the position of the data on the Jonker plots of the quadruple perovskite samples in Fig. 3 suggests a transition between intrinsic and extrinsic behavior, a defect model that neglects the contribution of electrons (Eq. [9]), i.e., $n \ll p$, does not adequately account for the transition from intrinsic to extrinsic character. Consequently, a modified model that accounts for the intrinsic due to electrons is required.

Modified Defect Model for Transitional Regime in Layered Perovskites

The Jonker pear represents different regions of intrinsic, extrinsic, or transitional behavior as conductivity increases. Therefore, the defect behavior of a semiconductor observed in its Brouwer plot should correspond with its Jonker behavior. Thus, a material whose data in the Jonker plot fall on the extrinsic region of the pear is expected to exhibit a corresponding extrinsic slope in its Brouwer plot. A plot that relates the expected Brouwer slope of undoped quadruple and quintuple perovskites to the location of their data in the Jonker plot (see description below) was proposed by Kane *et al.* (Fig. 7) (9). A modified version of that model for the aliovalently doped layered cuprates is proposed here.

Considering the same valid defect reaction of Eq. [3] and the common intrinsic electronic defect reaction,

$$\text{null} \leftrightarrow e' + h^{\bullet}, \qquad [10]$$

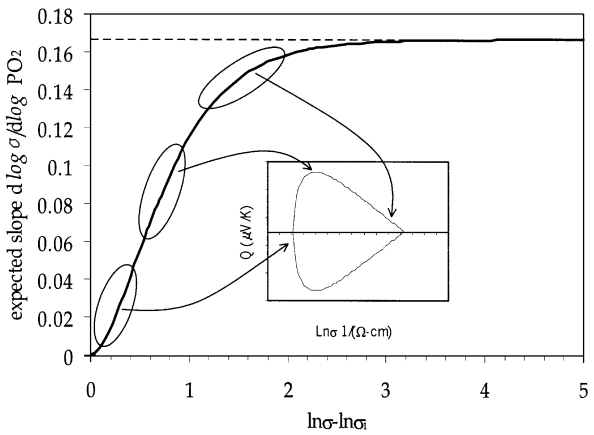

FIG. 7. The model for predicting defect mechanism for undoped layered cuprates, after Ref. (11).

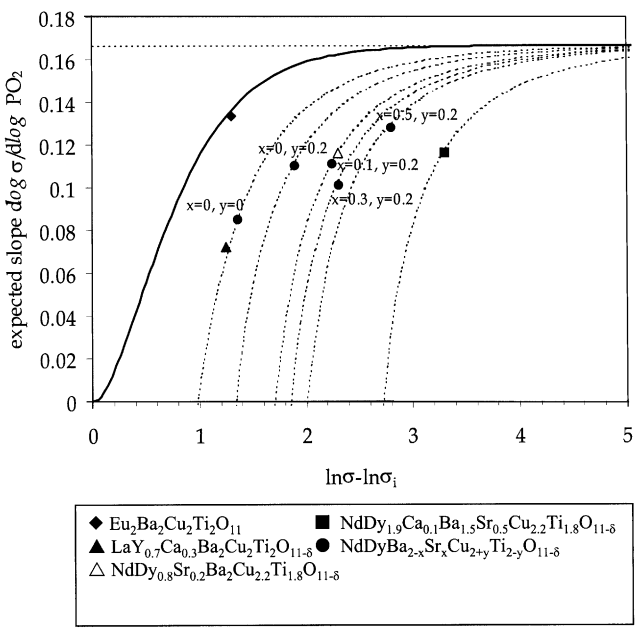

FIG. 8. The modified model for predicting defect mechanisms in doped layered cuprate perovskites. The dashed lines correspond to $c = 2.3$, 3.5, 5.3, 6.2, 7.3, and 15 from left to right.

results in the two defect equilibria:

$$K_{ox}P_{O_2}^{1/2} = [O_i'']p^2 \quad [11]$$

$$K_i = np. \quad [12]$$

Since the aliovalently doped layered perovskites in this study are mainly ionically compensated, a defect reaction that accounts for the impurity acceptors should be considered:

$$CuO + Ti_{Ti}^{\times} + O_O^{\times} \rightarrow Cu_{Ti}'' + V_O^{\bullet\bullet} + TiO_2. \quad [13]$$

This defect reaction, along with Eqs. [3] and [10], gives the general electroneutrality condition of

$$p + 2[V_O^{\bullet\bullet}] = n + 2[O_i''] + 2[Cu_{Ti}''] \quad [14]$$

If instead of isolated species (Eq. [13]), neutral associates form

$$CuO + Ti_{Ti}^{\times} + O_O^{\times} \rightarrow (Cu_{Ti}''V_O^{\bullet\bullet})^{\times} + TiO_2 \quad [15]$$

neither species ($[Cu_{Ti}'']$ or $[V_O^{\bullet\bullet}]$) will appear in the electroneutrality condition (Eq. [15]). The dopant, Cu_{Ti}'', is fully compensated in this case. However, if a portion of oxygen vacancies in associates can be refilled through oxygen annealing,

$$\frac{1}{2}O_2(g) + (Cu_{Ti}''V_O^{\bullet\bullet})^x \leftrightarrow O_O^x + Cu_{Ti}'' + 2h^{\bullet}, \quad [16]$$

this leaves some Cu_{Ti}'' species contributing to the extrinsic defect mechanism. Therefore, the general electroneutrality from Eq. [14] can be simplified to

$$p = n + 2[O_i''] + 2[Cu_{Ti}''] \quad [17]$$

Let $2[Cu_{Ti}''] = C$ and we have

$$[O_i''] = \frac{1}{2}(p - n - C). \quad [18]$$

Plugging this into the equilibrium condition of Eq. [11], we have

$$K_{ox}P_{O_2}^{1/2} = \frac{1}{2}(p - n - C)p^2. \quad [19]$$

This equation suggests an oxygen partial pressure dependence of holes and electrons that takes into account the aliovalent defect species, which is a more reasonable relationship for our defect regime than the one presented earlier. In order to interrelate the parameters in Eq. [19], a variable a is introduced such that $p = an_i$, where n_i is the intrinsic carrier concentration, and $n = a^{-1}n_i$ and $np = n_i^2$. Equation [19] can be rewritten as

$$K_{ox}P_{O_2}^{1/2} = \frac{1}{2}\left(an_i - \frac{n_i}{a} - C\right)a^2n_i^2. \quad [20]$$

We can relate C to intrinsic carrier concentration by assuming $C = cn_i$:

$$K_{ox}P_{O_2}^{1/2} = \frac{1}{2}an_i^3(a^2 - ca - 1). \quad [21]$$

The conductivity includes the contributions from both electrons and holes,

$$\sigma = ne\mu_e + pe\mu_h$$

$$\text{or } \sigma = e\mu(n + p), \quad [22]$$

if we assume (for simplicity) that the electrons and holes have similar mobilities (i.e., $\mu_e = \mu_h = \mu$). Substituting a into this equation gives:

$$\sigma = e\mu\left(an_i + \frac{1}{a}n_i\right) = e\mu n_i\left(a + \frac{1}{a}\right), \quad [23]$$

and since the intrinsic conductivity is $\sigma_i = 2n_ie\mu$, we have

$$\sigma = \frac{1}{2}\sigma_i\left(a + \frac{1}{a}\right). \quad [24]$$

The conductivity and intrinsic defect equilibrium expressions are now related to materials parameters by applying the a variable (Eqs. [21] and [24]). This allows us to establish a relationship between the expected slope in the Brouwer plot of $\log\sigma$-$\log pO_2$ and the corresponding defect regimes. In order to solve for $d(\log\sigma)/d(\log pO_2)$, i.e., the slope, we need to use the chain rule:

$$\frac{d\log\sigma}{d\log P_{O_2}} = \frac{d\log\sigma}{da}\frac{da}{d\log P_{O_2}}. \quad [25]$$

The logarithm of Eq. [24] is

$$\log\sigma = \log\left(\frac{1}{2}\sigma\right) + \log\left(a + \frac{1}{a}\right). \quad [26]$$

Taking the derivative of equation above with respect to a,

$$\frac{d\log\sigma}{da} = 0 + \left(a + \frac{1}{a}\right)^{-1}\left(1 - \frac{1}{a^2}\right) = \frac{a^2 - 1}{a(a^2 + 1)}. \quad [27]$$

Now, applying the same math steps, taking a logarithm and then derivative with respect to a, to the defect equilibrium Eq. [21]:

$$\log P_{O_2} = 2\log\left[\frac{1}{2}K_{ox}^{-1}an_i^3(a^2 - ca - 1)\right] \quad [28]$$

$$\frac{d\log P_{O_2}}{da} = 2\left[\frac{1}{a} + \frac{2a - c}{a^2 - ca - 1}\right]. \quad [29]$$

Plugging Eqs. [27] and [29] into the chain rule relation (Eq. [25]) gives the intended expression for the expected slope in Brouwer plots:

$$\frac{d\log\sigma}{d\log P_{O_2}} = \frac{(a^2 - 1)(a^2 - ca - 1)}{2(a^2 + 1)(3a^2 - 2ca - 1)}. \quad [30]$$

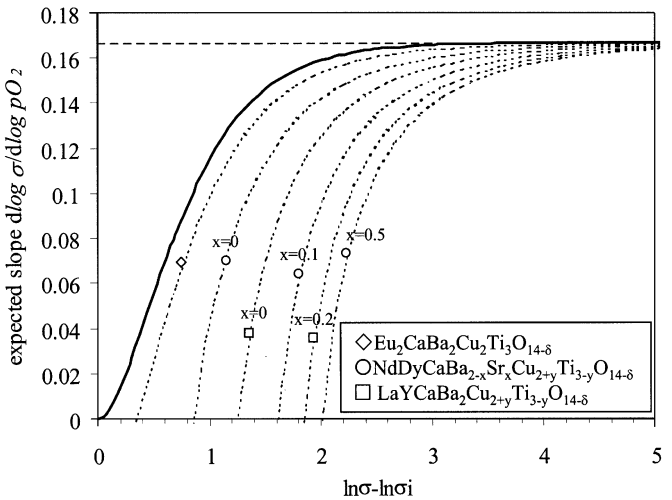

FIG. 9. The modified model for predicting defect mechanisms in doped layered cuprate perovskites. The dashed lines correspond to $c = 0.7$, 1.9, 3.2, 4.8, 6.2, and 7.3 from left to right.

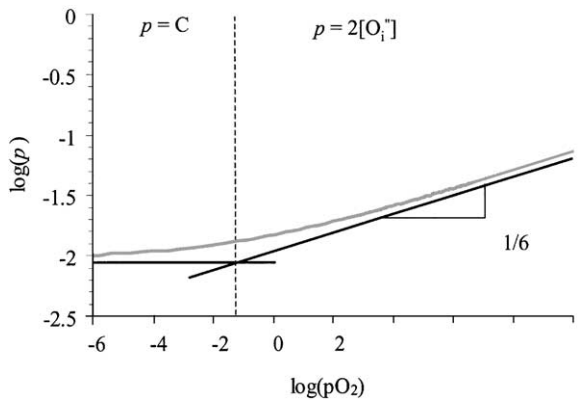

FIG. 10. Kröger–Vink diagram for two defect regimes in doped quadruple and quintuple perovskite layered cuprates.

Figure 7 plots $d(\log\sigma)/d(\log pO_2)$ vs $\ln\sigma - \ln\sigma_i$, i.e., Eq. [30] (where $c = 0$), as a function of $\ln(a)$ since

$$\ln\sigma - \ln\sigma_i = \ln\frac{\sigma}{\sigma_i} = \lim_{a\to\infty} \ln\frac{a^2+1}{a} = \ln a. \qquad [31]$$

Note that the intrinsic conductivity (σ_i) is where the Jonker plot crosses the $\ln\sigma$ axis (lowest conductivity point). The inset in Fig. 7 shows the corresponding regions of the Jonker plot for each portion of the curve. Figures 9 and 10 show the $d(\log\sigma)/d(\log pO_2)$ vs $\ln\sigma$–$\ln\sigma_i$ plot for the doped and undoped quadruple and quintuple compounds respectively from previous work and the present study based on the modified defect model presented above (9, 15, 25). The solid line in Fig. 7 is where $c = 0$ in Eq. [30]; i.e., oxygen interstitials are the dominant ionic defect species and Cu''_{Ti} species exist only in $[(Cu''_{Ti}V_O^{\bullet\bullet})^{\times}]$ neutral associates, while the curves with dashed lines correspond to different c values (c increases along the x-axis direction). The horizontal line at $d(\log\sigma)/d(\log pO_2) = \frac{1}{6}$ is the predicted slope for an extrinsically doped layered cuprate with electron holes dominating. Data points that have larger values along the x-axis in Fig. 8 exhibit data on the extrinsic leg of the Jonker pear, whereas the ones with smaller x value appear on the top of the pear (see Fig. 3), as in Fig. 9. The data that fall on the curves with larger c values indicate larger concentration of free dopant, $[Cu''_{Ti}]$. Larger values along the y-axis indicate more oxygen pressure sensitivity. The data for undoped quadruple and quintuple perovskites, $NdDyBa_2Cu_2Ti_2O_{11}$and $Eu_2CaBa_2Cu_2Ti_3O_{14-\delta}$, are expected to fall on the line with $c = 0$, but the deviation from the nominal stoichiometry can lead to a weak extrinsic doping.

A comparison within the family of $NdDyBa_{2-x}Sr_xCu_{2+y}Ti_{2-y}O_{11-\delta}$ and $NdDyCaBa_{2-x}Sr_xCu_{2+y}Ti_{3-y}O_{14-\delta}$ quadruple and quintuple perovskites in Figs. 8 and 10 (data for different x and y values are labeled in the plot) confirms an increase in carrier content as a result of aliovalent doping. Data for this series of samples fall on the curves with larger values of c as x and y increase, implying an improvement in the hole content as Sr level increases. This agrees with the earlier observations of oxygen content increase in these materials by Sr substitution in the previus work. The fact that the data for the undoped $NdDyBa_2Cu_2Ti_2O_{11}$ quadruple compound falls on the curve with lowest c and in the lower portion of the plot compared to the rest of NdDy quadruple family corroborates the Jonker analysis results with the data on the top of the curve and the lowest conductivity among all the species (25). The C value for the compounds with A- and B-site codoping corresponds to the sum of concentrations of aliovalent dopants (e.g., $[Sr'_{Dy}] + [Cu''_{Ti}]$).

The only datum that falls on the $c = 0$ curve (oxygen interstitial domination with no extra holes) is $Eu_2Ba_2Cu_2Ti_2O_{11}$, a compound from a previous work which is an undoped quadruple compound with poor electrical properties, as evidenced in its Jonker plot (27). This compound has a large–large A-cation combination that allows for excessive oxygen interstitial intercalation between Cu–O sheets. The Jonker plot for $Eu_2Ba_2Cu_2Ti_2O_{11}$ compound shows its data falling on the top of the pear.

The data point with the highest c value is for the $NdDy_{1.9}Ca_{0.1}Ba_{1.5}Sr_{0.5}Cu_{2.2}Ti_{1.8}O_{11-\delta}$ quadruple compound. This material has the best electrical properties in Jonker analysis, slow-cooling experiments, and low-temperature resistivity measurements (see Figs. 4, 5). The material with the lowest slope in Fig. 5 belongs to the A-site doped $LaY_{0.7}Ca_{0.3}Ba_2Cu_2Ti_2O_{11-\delta}$ quadruple compound, whose Jonker data fall on the top and upper part of the extrinsic leg of the pear.

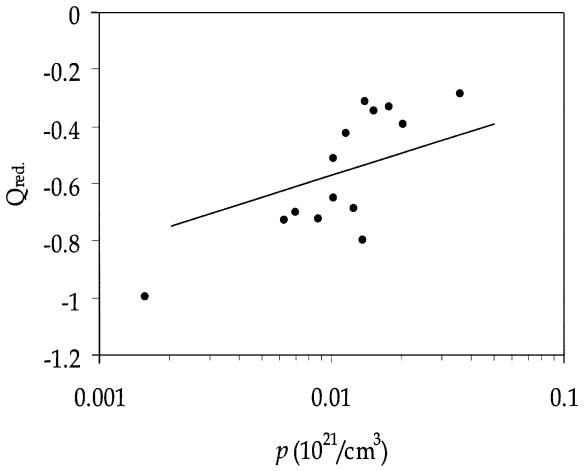

FIG. 11. Plot of reduced thermopower vs logarithm of p at 700°C for the quadruple compounds in Fig. 8.

Estimation of Effective Dopant Level

An important result of the model presented in the previous section is that c values fitted to each data point in Figs. 9 and 10 can provide information about the concentration of effective acceptor dopants in these materials. The following mathematical calculations allow the concentration of free Cu''_{Ti} to be determined. The effective dopant concentration calculated on the basis of this model is the effective hole concentration (p) in these bond-matched structure materials.

We assumed earlier that intrinsic carrier content is related to $[Cu''_{Ti}]$ by $C = cn_i$. Intrinsic carrier concentration is defined as (16)

$$n_i = N \exp\left(\frac{-E_g}{2kT}\right), \qquad [32]$$

where N is the density of states, E_g is the band gap, k is the Boltzmann's constant, and T is the absolute temperature. A normalized C for each compound can be determined, based on the quadruple compound that has the largest c, if the density of states is assumed to be constant in these compounds:

$$\frac{c_x}{c_{x_o}} = \frac{\dfrac{C_x}{n_{i(x)}}}{\dfrac{C_{x_o}}{n_{i(x_o)}}} = \frac{C_x}{C_{x_o}} \frac{N_{x_o}}{N_x} \frac{\exp\left(\dfrac{-E_{g(x_o)}}{2kT}\right)}{\exp\left(\dfrac{-E_{g(x)}}{2kT}\right)}. \qquad [33]$$

Simplifying,

$$\frac{C_x}{C_{x_o}} = \frac{c_x}{c_{x_o}} \exp\left(\frac{E_{g(x_o)} - E_{g(x)}}{2kT}\right). \qquad [34]$$

Another way of expressing the percentage of free acceptor dopant concentration in these materials is based on the observed thermopower values of known superconductors. A 10% hole doping in $La_{2-x}Ba_xCuO_4$, $La_{2-x}Sr_xCuO_4$, and $Bi_{2.1}Sr_{1.9}(Ca_{1-x}Y_x)Cu_2O_y$ layered cuprate high-T_c superconductors corresponds to $Q \cong 19$–21 μV/K in their Jonker analysis (5, 6, 28). The corresponding $\ln \sigma$ for $Q = 20$ μV/K in a Jonker measurement can be then used for a simple calculation of n_i, where $\sigma_i = 2n_i e\mu$ and $\sigma_{[Q=20\mu V/K)]} = Ce\mu$:

$$\frac{\sigma_i}{\sigma_{(Q=20\,\mu V/K)}} = \frac{2n_i e\mu}{Ce\mu} = \frac{2n_i}{C}. \qquad [35]$$

Because C and n_i have the same (cm^{-3}) units, new unitless C' and n'_i terms will be used for simplifying Eq. [35]:

$$\frac{\sigma_i}{\sigma_{(Q=20\,\mu V/K)}} = \frac{2n_i}{C} = \frac{2n'_i F}{C' F} = \frac{2n'_i}{0.1}, \qquad [36]$$

where F is the number of Cu sites per cubic centimeter and $C' = 0.1$ ($\sim 10\%$ doping level at $Q = 20$ μV/K). σ at $Q = 20$ μV/K and σ_i are taken from the Jonker pear fit for each sample in Fig. 8, n'_i is calculated from Eq. [36], n_i is calculated from the $n'_i F = n_i$ relationship, and C is then the product, cn_i (c is the fit parameter for the corresponding data point in Fig. 8). Table 3 tabulates the calculated C (effective dopant concentration) for the quadruple and quintuple compounds in Figs. 9 and 10. The unit for C is the number of copper sites per cubic centimeter which is calculated on average to be about $10^{20}/cm^3$ in the quadruple compounds in the present study. The $NdDy_{0.9}Ca_{0.1}Ba_{1.5}Sr_{0.5}Cu_{2.2}Ti_{1.8}O_{11-\delta}$ compound with the best Jonker analysis results among other quadruples in the present study (see Fig. 3) has the highest estimated effective dopant level (0.036). The concentrations of free dopant species in Table 3 are calculated from C since $C = 2[Cu''_{Ti}]$, $[Ca'_Y]$, $[Ca'_{Dy}] + 2[Cu''_{Ti}]$, or $[Sr'_{Dy}] + 2[Cu''_{Ti}]$ in the doped quadruple and quintuple compounds. Therefore, C is divided by 2 for the Cu B-site doped quadruples, whereas for the A- and B-sites codoped quadruple compounds, a range of effective dopant levels is given in Table 3 because it is not clear which acceptor species (e.g., $[Ca'_{Dy}]$ or $[Cu''_{Ti}]$ in $NdDy_{0.9}Ca_{0.1}Ba_{1.5}Sr_{0.5}Cu_{2.2}Ti_{1.8}O_{11-\delta}$ compound) is the dominant free dopant.

A comparison between the effective dopant concentrations of quadruple and quintuple perovskite compounds in this study suggests insignificant differences. This implies that the superior conductivity and thermopower behavior of quadruple compounds compared to the quintuple compounds are due to the structural rather than electronic features of these structures (e.g., shorter blocking layers, structural motifs allowing oxygen vacancy refilling).

The C values in Table 3 are lower than the TGA-derived hole contents (p') in Table 2 which are calculated according to Eq. [4] and do not consider the presence of neutral associates. In other words, the $[Cu''_{Ti}]$ term in Eq. [4] is the total concentration of that species and not the free $[Cu''_{Ti}]$

TABLE 3
Calculated Hole Content (p) and Effective Dopant Concentration in Quadruple Perovskites

Compound	σ_i $(\Omega cm)^{-1}$	$\sigma_{(Q=20)}$ $(\Omega cm)^{-1}$	n_i'	c	C or p $(10^{20}/cm^3)$	Effective Dopant $(10^{20}/cm^3)$
$Eu_2Ba_2Cu_2Ti_2O_{11}$	0.741	21.0	0.0017	0.1	0.0002	—
$NdDyBa_2Cu_2Ti_2O_{11}$	0.301	4.9	0.0031	2.3	0.007	—
$NdDyBa_2Cu_{2.2}Ti_{1.8}O_{11-\delta}$	4.263	63.8	0.0033	3.5	0.012	0.006
$NdDyBa_{1.9}Sr_{0.1}Cu_{2.2}Ti_{1.8}O_{11-\delta}$	3.320	86.0	0.0019	5.3	0.010	0.005
$NdDyBa_{1.7}Sr_{0.3}Cu_{2.2}Ti_{1.8}O_{11-\delta}$	3.669	63.5	0.0029	6.2	0.018	0.009
$NdDyBa_{1.5}Sr_{0.5}Cu_{2.2}Ti_{1.8}O_{11-\delta}$	2.117	55.2	0.0019	7.3	0.014	0.007
$NdDy_{0.8}Sr_{0.2}Ba_2Cu_{2.2}Ti_{1.8}O_{11-\delta}$	4.055	70.5	0.0029	5.3	0.015	0.0075–0.015
$NdDy_{0.9}Ca_{0.1}Ba_{1.5}Sr_{0.5}Cu_{2.2}Ti_{1.8}O_{11-\delta}$	4.481	93.0	0.0024	15.0	0.036	0.018–0.036
$LaY_{0.7}Ca_{0.3}Ba_2Cu_2Ti_2O_{11-\delta}$	6.049	34.0	0.0089	2.3	0.021	0.021
$NdCaDyBa_2Cu_{2.2}Ti_{2.8}O_{14-\delta}$	1.9155	28.9	0.0033	1.9	0.0063	0.0031
$NdCaDyBa_{1.9}Sr_{0.1}Cu_{2.2}Ti_{2.8}O_{14-\delta}$	1.6160	38.0	0.0021	4.8	0.0102	0.0051
$NdCaDyBa_{1.5}Sr_{0.5}Cu_{2.2}Ti_{2.8}O_{14-\delta}$	0.2725	7.9	0.0017	7.3	0.0125	0.0062
$LaYCaBa_2Cu_2Ti_3O_{14-\delta}$	0.9802	11.5	0.0042	3.2	0.0136	—
$LaYCaBa_2Cu_{2.2}Ti_{2.8}O_{14-\delta}$	0.5945	21.0	0.0014	6.2	0.0088	0.0044
$Eu_2CaBa_2Cu_2Ti_3O_{14-\delta}$	0.3867	8.6	0.0022	0.7	0.0016	—

species,

$$[Cu''_{Ti}]_{total} = [Cu''_{Ti}] + [(Cu''_{Ti}V_O^{\bullet\bullet})^{\times}]. \qquad [37]$$

The C values (the third term in Eq. [17]) can be a close estimation of the effective carrier content (p), if the concentration of n and $[O_i'']$ are negligible in Eq. [17]. A Kröger–Vink plot for the doped quadruple layered cuprate materials in Fig. 10 allows a good estimation of the oxygen interstitial concentration. The transitional regime between the zero and 1/6 slope in Fig. 10 (slope $\sim \frac{1}{9}$–$\frac{1}{12}$) corresponds to the defect regime of the quadruple compounds in the present study (see Fig. 5).

Simplifying Eq. [17] by neglecting the electron concentration in the extrinsic defect regime,

$$p = 2[O_i''] + 2[Cu''_{Ti}] \qquad [38]$$

we can find the relationship between the p and pO_2 by substituting for the first term of the equation above from Eq. [11], where $[O_i''] = [Cu''_{Ti}]$ (an assumption for simplification):

$$pO_2^{1/2} = \frac{p^3 - Cp^2}{2K_{ox}}. \qquad [39]$$

K_{ox} can be estimated in the transitional regime, where $C = 2[Cu''_{Ti}] \sim 0.01$ and pO_2 is in an intermediate range (10^{-3}–10^{-2}) according to Eq. [11] ($K_{ox} \sim 10^{-8}$). The estimated K_{ox} can then be used for the calculation of a range of p and pO_2 values according to Eq. [39] using a computer spreadsheet. The result of this calculation shows $p \sim 0.0135$–0.0175 for slopes of 1/12–1/9 in the Kröger–Vink plot (the transitional regime between $p = C$ and $p = 2[O_i'']$ in Fig. 10). These values for p indicate an oxygen interstitial concentration less than or comparable to C (the effective dopant concentration). Therefore, the effective hole concentration in Eq. [38] is slightly higher than the calculated value of C as the slope in the Brouwer plot decreases (i.e., less oxygen sensitivity). The reduced thermopower, Q_{red}, which is a linear function of the hole concentration according to

$$Q_{red} = -\frac{Q}{k/e} = \ln p - \ln N_v - A, \qquad [40]$$

is plotted vs logarithm of C in Fig. 11 at 700°C and 1 atm pO_2 for these quadruple compounds. The data in Fig. 11 correspond to the same quadruple compounds in Fig. 8. The slope of the line in the plot is unity. The nearly linear behavior of the data in the Q_{red} vs C plot supports the carrier content estimation argument based on the presented defect model (i.e., reduced thermopower increases as the hole content increases).

A master plot of the high-temperature Seebeck coefficients (Q) of various known layered cuprate superconductors vs hole concentration, presented previously, provides a useful means to evaluate the potential of new materials for superconductivity (Fig. 12) (15). The hole concentrations were calculated on the basis of the oxygen content data in the literature (4, 7, 29–32). The Seebeck coefficients were measured under flowing oxygen at $\sim$700°C (1, 3, 5, 6, 8, 33). The solid lines in Fig. 12 refer to a rough boundary of the region containing all the data known for superconducting layered cuprates. The dashed line separates the superconducting from non-superconducting region. Some data for quadruple perovskites from the present study fall to the right of the boundary in the superconducting regime (such

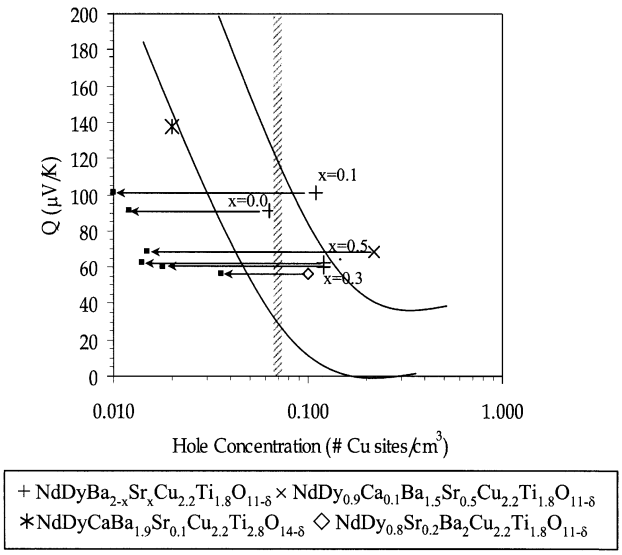

FIG. 12. Master plot of Seebeck coefficient–hole concentration with some data from the present study. The Sr levels in the $NdDyBa_{2-x}Sr_xCu_{2.2}Ti_{1.8}O_{11}$ series are labeled on the plot. The arrows show the data for the corresponding compound when the effective hole concentration (C) is used instead of TGA-derived hole concentration.

as the $NdDyBa_{1.5}Sr_{0.5}Cu_{2.2}Ti_{1.8}O_{11-\delta}$ and $NdDy_{1.9}Ca_{0.1}Ba_{1.5}Sr_{0.5}Cu_{2.2}Ti_{1.8}O_{11-\delta}$ materials) when the TGA-derived hole content (p') is used, as shown in Fig. 12. This indicates that carrier concentrations necessary for superconductivity have been achieved in these materials; nevertheless, they are not superconducting, as evidenced by low-temperature magnetic susceptibility and resistivity measurements. However, if the effective dopant concentration (C), calculated on the basis of the modified defect model, is used in the master plot in Fig. 12 (as shown by arrows), none of the quadruple or quintuple layered cuprate perovskites fall in the superconducting region, implying an underdoped layered cuprate structure. A more precise estimation of the oxygen interstitial concentration, based on the earlier discussion, implies that using the effective hole content (p) instead of C in Fig. 12 does not significantly shift the data toward the right.

CONCLUSION

Large–small A-cation combinations (e.g., NdDy and LaY) for Ti-blocking layer quadruple perovskites in the present and previous work produced a wide range of compounds with most of the essential structural features for superconductivity. Applying structural and electronic modifications by A- and/or B-site aliovalent and isovalent substitutions in $NdDy_{1-z}AE_zBa_{2-x}Sr_xCu_{2+y}Ti_{2-y}O_{11-\delta}$ (AE = Sr or Ca) and $LaY_{1-x}Ca_xBa_2Cu_{2+y}Ti_{2-y}O_{11-\delta}$ quadruple systems yielded improved doping and electrical/transport properties, as evidenced in the TGA, Jonker analysis, and electrical resistivity measurements. Some of the compounds showed high-temperature thermopower and conductivity values close to the threshold values for superconductivity at different temperatures and oxygen partial pressures. A transition from semiconductor to metallic behavior was observed in the high-temperature slow-cooling measurements (conductivity, thermopower) and in the low-temperature resistivity measurements.

Because the bond length mismatch in Ti-blocking layer quadruple perovskites is not sufficient for introducing enough carrier into the system, ionic compensation dominates, rather than electronic compensation, upon acceptor or donor doping, inhibiting superconductivity in these structures. Although TGA results confirmed an increased oxygen content in some of the chemically and structurally doped NdDy and LaY quadruple samples, electrical measurements did not show sufficient hole or electron carrier density in these systems.

A defect model based on the location of the data on the Jonker plot (thermopower vs conductivity) and the slope in the Brouwer plot (conductivity vs oxygen partial pressure) of a doped quadruple or quintuple layered cuprate perovskite allows for calculation of effective dopant level in these materials. A straightforward calculation of effective dopant level in a number of aliovalently doped quadruple perovskites showed only 2.1% or less (based on $\sim 10^{20}/cm^3$ Cu sites) of effective dopant species.

REFERENCES

1. M. Y. Su, E. A. Cooper, C. E. Elsbernd, and T. O. Mason, *J. Am. Ceram. Soc.* **73,** 3453 (1990).
2. A. M. Stoneham and L. W. Smith, *J. Phys.* **3,** 225 (1991).
3. "Defect Chemistry of High T_c Superconducting Cuprates" (T. O. Mason, Ed.) Trans. Tech. Publications, Zurich, 1992.
4. J. D. Jorgensen, *Phys. Today* 34 (1991).
5. B. Hong and T. O. Mason, *J. Am. Ceram. Soc.* **76,** 635 (1993).
6. D. J. L. Hong and D. M. Smyth, *J. Solid State Chem.* **102,** 250 (1993).
7. L. Shen, P. A. Salvador, and T. O. Mason, *J. Am. Ceram. Soc.* **77,** 81 (1994).
8. L. Shen, P. A. Salvador, and T. O. Mason, *J. Phys. Chem. Solids* **57,** 1311 (1996).
9. M. H. Kane, N. Mansourian-Hadavi, T. O. Mason, W. Sinkler, L. D. Marks, K. D. Otzchi, D. Ko, and K. R. Poeppelmeier, *J. Solid State Chem.* **148,** 3 (1999).
10. J. B. Goodenough and A. Manthiram, *J. Solid State Chem.* **88,** 115 (1990).
11. R. D. Shannon, *Acta. Crystallogr. A* **32,** 751 (1976).
12. D. L. Novikov, A. J. Freeman, and K. R. Poeppelmeier, *Phys. Rev. B* **53,** 9448 (1996).
13. M. R. Palacin, N. Casan-Pastor, and P. Gomez-Romero, *J. Solid State Chem.* **138,** 141 (1998).
14. P. Gomez-Romero, M. R. Palacin, C. R. Michel, and N. Casan-Pastor, *Solid State Ionics* **101–103,** 411 (1997).
15. N. Mansourian-Hadavi, D. Ko, T. O. Mason, and K. R. Poeppelmeier, *J. Solid State Chem.* **155,** 216 (2000).
16. G. H. Jonker, *Philips Res. Rep.* **23,** 131 (1968).
17. M. Su, C. E. Elsbernd, and T. O. Mason, *J. Am. Ceram. Soc.* **73,** 415 (1990).

18. G. Brouwer, *Phillips Res. Rep.* **9,** 366 (1954).
19. B. S. Hong, "Materials Scince," 142. Northwestern University, Evanston, IL, 1994.
20. A. LeBail, H. Duroy, and J. L. Fourquet, *Mater. Res. Bull.* **23,** 447 (1988).
21. A. C. Larson and R. B. V. Dreele, National Laboratory Neutron Scattering Center, Los Alamos, NM, 1985.
22. P. A. Salvador, L. Shen, T. O. Mason, K. B. Greenwood, and K. R. Poeppelmeier, *J. Solid State Chem.* **119,** 80 (1995).
23. A. Trestman-Matts, S. E. Dorris, and T. O. Mason, *J. Am. Ceram. Soc.* **66,** 589 (1983).
24. D. S. McLachlan, M. Blaszkiewicz, and R. E. Newnham, *J. Am. Ceram. Soc.* **73,** 2186 (1990).
25. P. A. Salvador, T. O. Mason, K. Otzschi, K. B. Greenwood, K. R. Poeppelmeier, and B. Dabrowski, *J. Am. Chem. Soc.* **119,** 3756 (1997).
26. K. B. Greenwood, G. M. Sarjeant, K. R. Poeppelmeier, P. A. Salvador, T. O. Mason, B. Dabrowski, K. Rogacki, and Z. Chen, *Chem. Mater.* **7,** 1355 (1995).
27. P. A. Salvador, "Materials Science," 242. Northwestern University, Evanston, IL, 1997.
28. "High Temperature Defect Structure and Transport in RareEarth-Alkaline Earth-Copper Oxide Superconductors" (M. Su, Y. K. Sujata, and T. O. Mason, Eds.). Am. Cer. Soc., Westerville, OH, 1988.
29. E. J. Opila and H. L. Tuller, *J. Am. Ceram. Soc.* **77,** 2727 (1994).
30. E. Takayama-Muromachi and D. E. Rice, *Physica C* **177,** 195 (1991).
31. C. Rial, E. Moran, M. A. Alario-Franco, U. Amador, J. L. Martinez, J. Rodrigues-Carvajal, and N. H. Andersen, *Physica C* **297,** 277 (1998).
32. W. A. Groen, D. M. d. Leeuw, and L. F. Feiner, *Physica C* **165,** 55 (1990).
33. B.-S. Hong and T. O. Mason, *J. Mater. Res.* **6,** 2054 (1991).